Chapter 1: Introduction and Literature Review

1.1. Background and Motivation

Nowadays, microwaves (30 – 300 GHz) are playing an important role in the day-to-day routine in our society. There are very few sources available that produce high power in such a high-frequency range. Microwave tubes are capable of producing high power at high frequencies. The use of microwave tubes is ubiquitous, ranging from ground-based to deep-space communications, civil and defense requirements, space exploration, strategic industrial applications, generation of thermonuclear energy, and so on [1] – [8]. The microwave tubes are proving vacuum-based electronic devices, which are very useful in many fields such as radar, plasma heating in fusion research, medical imaging, materials processing, advanced particle accelerators, etc. [9] – [13]. In addition, the microwave tubes are operated in millimeter-wave range and extend their applications, including high-resolution radars, high information density communications, plasma diagnostics, advanced satellite communications, chemistry, and high energy physics, advanced high gradient RF linear particle accelerators, laser pumping, nonlinear spectroscopy, electron cyclotron resonance (ECR) heating of fusion plasmas, high power microwaves (HPM) electronic warfare and imaging in atmospheric and planetary science, etc. [14] – [23].

The development of solid-state technology in the early 1970s saw a strong rise of solid-state sources in the microwave regime. However, vacuum electron devices (VEDs), also known as microwave tubes, have the unique ability to produce several orders of power than the solid-state sources (SSDs) in the microwave and millimeter-wave regimes. The small size of semiconductor devices limits their power handling capability, while the VEDs have no restrictions on size and can provide higher output power with higher power handling capability [1], [9]. The promise of a wide bandgap of semiconductor transistors for high-power applications has yet to be materialized. Many examples can

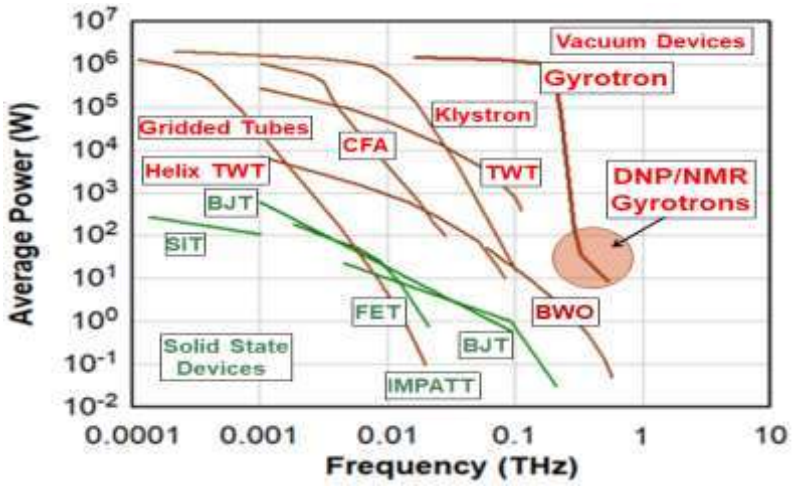

Figure 1.1 Comparison of average power versus frequency for various types of devices [24].

be cited of the eventual rescue of VEDs. Where the solid-state power sources and amplifiers could not meet the final specifications in some military systems, and how VEDs such as inductive output tubes and highly efficient amplifiers are preferred over solid-state devices [1].

The progress in RF vacuum electronics was proposed in different types of devices based on the evaluation of power density, which provides a basis for accurate comparison of different types of devices in the form of a figure of merit. The superior performance of VEDs as compared to SSDs in terms of power density and frequency can be seen in Figure 1.1, which shows the state-of-the-art of microwave and submillimeter-wave sources [24]. Any device's physical significance is based on the fact that the maximum beam power can be carried through the device, which is directly proportional to the circuit's cross-sectional area, *i.e.* inversely proportional to the operating frequency. As the operating frequency of the device increases, the power handling capacity of the devices decreases significantly. Meanwhile, superconducting magnets' development gave birth to a new class of microwave devices (fast-wave devices) to meet some new necessities. The fast-wave devices including gyro-monotron

or simply called gyrotron, gyro traveling-wave tube (gyro-TWT), gyro backward-wave oscillator (gyro-BWO), gyro-klystron, and gyro-twystron [25] – [26].

Some new applications such as Dynamic Nuclear Polarization / Nuclear Magnetic Resonance (DNP / NMR) spectroscopy, high-frequency communications, and radar have increased the device operation's demand at higher frequencies. It now pushed the research and development towards the electromagnetic spectrum of millimeter-wave, sub-millimeter-wave, and terahertz (THz) regimes. Among all the above applications, the DNP / NMR spectroscopy is the most exciting application that requires a frequency-tuneable microwave source to produce a few tens of watt power in millimeter-wave, submillimeter-wave, and THz regime for a long period of operation [27].

LASER cannot deliver high power beyond the mid-infrared region, and conventional RF sources face severe problems due to the inverse frequency scaling of their components [1]. At such high frequencies (0.1 – 1 THz), microwave tubes are the only available sources to provide continuous power because their solid-state counterparts cannot compete at such high frequencies. Among the entire microwave tubes, the gyrotron oscillator based on the electron cyclotron resonance maser instability is the most promising source that can generate CW power in millimeter-wave, sub-millimeter wave, and THz regime. The gyrotron oscillator can provide sufficient power (a few tens of watts) for a long period of ~ 50,000 hours in the required frequency range of DNP / NMR applications due to the use of overmoded interaction cavities in the gyrotron [27].

The most important point is that the DNP technique requires a frequency-tuneable gyrotron to optimize the frequency matching conditions between nuclear spin and

electron spin. Maintaining both broadband frequency tuning and high efficiency is the major

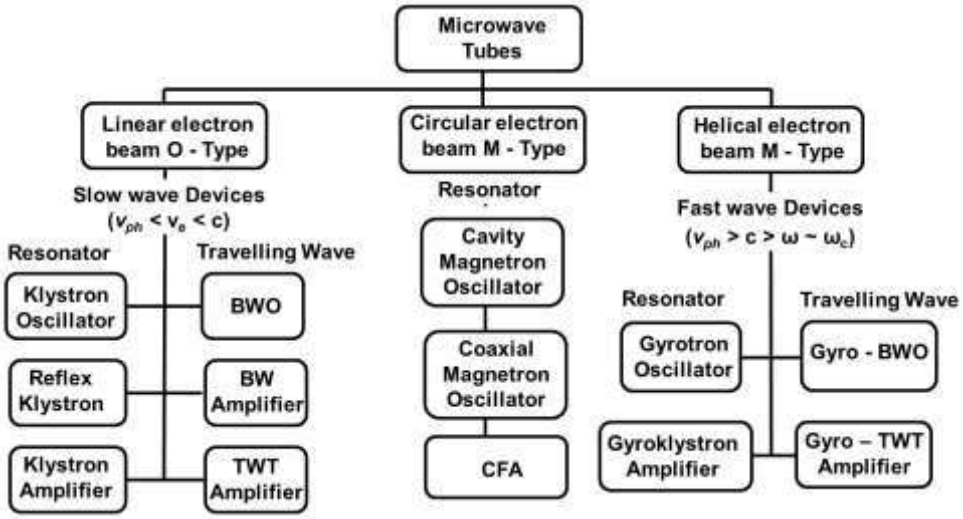

Figure 1.2 Classification chart of vacuum electron devices [1].

challenges for high-frequency gyrotrons in DNP / NMR experiments. It's motivated the author of the present thesis to work in high-frequency gyrotrons, in which the author has attempted to maintain broadband frequency tuning of gyrotrons in millimeter-wave and submillimeter-wave regimes.

1.2. Classification of Microwave Tubes

Microwave tubes can be classified based on the propagation of the electron beam and the device's operating principle, as shown in Figure 1.2. This is achieved by bunching electrons in the proper phase regarding the electromagnetic (EM) wave in the RF interaction structure. Different approaches to classify the microwave tubes are well described in the literature [1], [9], [17], [25]. Microwave tubes are classified as O-type (O is French acronym of TPO which stands for tubes à propagation desondes) and M-type (M is the acronym of TPOM standing for tubes à propagation des ondes à champs magnetique) tubes. The O-type tubes are also known as linear beam devices in which

the electron beams propagate in the longitudinal direction due to a DC magnetic field in the same direction and interact with a longitudinal electric field supported by the interaction RF circuit. In the O-type tubes, the electron beam transfer of axial kinetic energy to the RF wave occurs. The M-type tube is also known as a cross-field device in which the electron beam propagates in a direction perpendicular to the DC electric field and magnetic field. In this type, the transverse kinetic energy of the electron beam is transferred to the RF wave. Traveling wave tubes and klystrons are well-known examples of O-type devices, while magnetron and cross-field amplifiers (CFAs) are examples of M-type tubes.

The classification of microwave tubes is based on another process in which particles can produce electromagnetic radiation: Cherenkov radiation, transition radiation and bremsstrahlung radiation. In Cherenkov radiation type, the electron beam propagates in a medium or structure with a velocity higher than the RF wave's phase velocity. Backward wave oscillators (BWOs), traveling-wave tubes (TWTs), cross-field amplifiers (CFAs), magnetrons, and orotrons are famous examples of Cherenkov radiation-based microwave tubes. In transition radiation type, electrons travel through spatial inhomogeneous media such as media with different refractive indices or perturbations, including conducting grids, plates, or gaps between conducting surfaces. Klystron is an example of this type of radiation. In the bremsstrahlung radiation type, the electron emits the radiation while accelerating/decelerating in an external electric field or magnetic field. This type of radiation occurs in gyrotrons, ubitrons, peniotrons, FELs, and virtual cathode oscillators (VIRCATORs). Another criterion based on the velocity of the electron beam and the RF wave's phase velocity, microwave tubes can be classified into slow-wave or fast-wave devices. The conversion of electron beam energy

(kinetic or potential) into an RF wave is also a criterion for classifying a microwave tube.

Slow-wave devices such as Klystron, TWT, and BWO all have tiny interaction structures (resonant cavities and helix) on the order of wavelength. As the operating frequency increases, the device size decreases, which leads to a severe problem in the manufacturing of slow-wave devices at such a high frequency. The device's small size also limits its power handling capability or current density before ohmic heating or arcing, resulting in the device's failure. The lifetime of slow-wave devices is also reduced due to electron beam interception. As a result, slow wave devices' operation is limited to less than ~100 GHz operating frequency, as shown in Figure 1.1.

Fast-wave devices such as gyrotron oscillator (gyromonotron), gyrotron backward wave oscillator (gyro-BWO), gyrotron travelling-wave tube (gyro-TWT), and gyro-twystron have large size interaction structure that can enhance the power handling capability of the devices. As the frequency increases, the transverse amplitude of the fast-wave devices' intermittent structure decreases like that of slow-wave devices. However, the transverse dimension reduction of the interaction structure is much greater in slow-wave devices than in fast-wave devices. The transverse dimension of the interaction structure can be further increased by operating the fast-wave devices in higher-order transverse electric (TE) mode. As fast-wave devices, Gyrotron oscillators can overcome the problem of power handling capability in millimeter wave, sub-millimeter wave, and THz regime.

1.3. Gyrotron Oscillator

The design of gyrotron was first reported in 1963 and tested in the following year in 1964 with an output power of 6 W in continuous-wave (CW) at 10 GHz [9]. Considerable RF power with very good efficiency was observed in this test compared to

the previous experiments. This test's operation was performed successfully in 1964 by Heerfield and Wachtel [28] in the United States. Gyrotron oscillator is an efficient high power microwave and millimeter-wave radiation source (oscillator) based on CRM instability. The RF behavior of gyrotron has been well investigated theoretically and experimentally, as evident from previous studies [1], [9], [17], [25], [29] – [31].

1.3.1. Dispersion Relation

The device's operational characteristic is controlled by the dispersion relation and the device synchronization state that can be obtained at the grazing intersection between the beam mode and the waveguide mode dispersion curves [1], [25]. In a cyclotron period, the beam mode dispersion relation can be obtained using the concept of completing one or more RF cycles [25]. Waveguide-mode dispersion relation can be determined by considering a TE_{mn} mode propagating in the axial direction (z-direction) of a cylindrical waveguide. The beam mode dispersion relation represents the gyrating electron beam, $\omega - s\omega_c - k_z v_z = 0$, and the waveguide-mode dispersion for TE_{mn} mode are represented by $\omega^2 - k_z^2 c^2 - k_\perp^2 c^2 = 0$, where, ω is the angular frequency, $\omega_c = eB_o / \gamma m_e$ is the cyclotron angular frequency, v_z is the axial velocity of electron beam, k_z is axial propagation constant, $k_\perp$ is transverse propagation constant, s is the harmonic number, and c is the free space velocity of light. The velocity of the light line is represented by $\omega = c k_z$. The intersection of the beam mode line and the waveguide mode curve is described by the above equations that provide the synchronism condition. These dispersion relations for the gyrotron oscillators are given in Figure 1.3, which provides clear information about their operating conditions. Gyrotron is generally

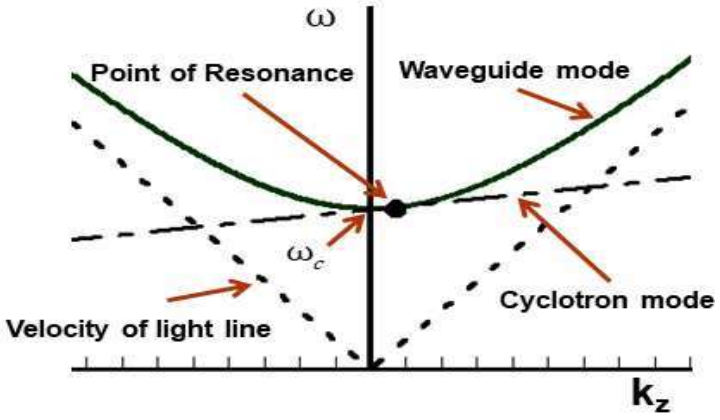

Figure 1.3 Dispersion diagram of gyrotron oscillator.

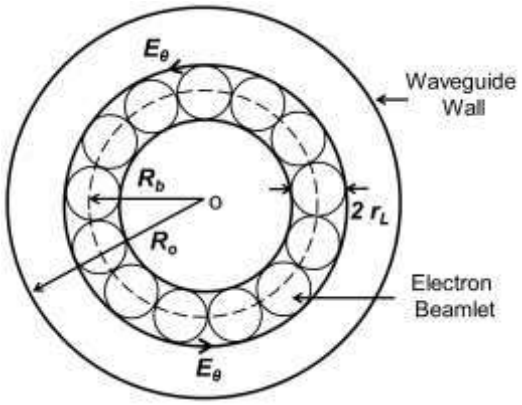

Figure 1.4 RF electric field of TE_{0n} mode with electron beamlets.

operated close to the waveguide cut-off frequency at near-zero group velocities. This significantly slows the beam's velocity to maintain the electromagnetic energy in the wave resonance cavity for the interaction with the electron beam.

1.3.2. CRM Interaction Mechanism

Instability in beam-wave systems can be of many types. Their operation is mainly based on the interaction of electromagnetic waves and slow and fast space-charge waves of the electron beam in an interaction structure. The process of energy extraction is distinctive among all the instabilities. In the presence of a DC magnetic field, the interaction between the gyrating electron beam and the electromagnetic wave causes the extraction of the electron beam's transverse kinetic energy. This type of

interaction is known as CRM instability [10], which occurs in the gyrotron. The numerical explanation given in the previous section shows the synchronism between the transverse electric waveguide mode and the electron beam that depends on the cyclotron frequency and the relativistic mass factor. The relative cyclotron frequency depends on the electron's energy due to CRM instability.

The arrangement of electron beamlets in the process of CRM interactions is shown in Figure 1.4. An annular electron beam is assumed to be in the waveguide submerged in a background axially stable magnetic field B_o [1]. In Figure 1.4, R_o is the waveguide radius, and R_b is the beam radius, which is also known as the guide center radius of the beamlets. The field orientation of the TE_{0n} mode is shown in Figure 1.4. The beam thickness is equal to twice the Larmor radius (r_L), which is defined as

$$r_L = \frac{v_\perp}{\omega_c} \tag{1.1}$$

where, $v_\perp$ is the transverse velocity. The relativistic mass factor (γ), in terms of axial velocity (v_z) and transverse velocity ($v_\perp$), is defined as,

$$\gamma = \left(1 - \left(v_\perp^2 + v_z^2\right)/c^2\right)^{-1/2} \tag{1.2}$$

The cyclotron angular frequency (ω_c) is defined as,

$$\omega_c = \frac{e B_o}{\gamma m_e} \tag{1.2}$$

The azimuthal component of the RF electric field (E_θ) interacts with the electron beam in the transverse plane and in which the alteration of the relativistic factor (γ) causes a change in the relativistic cyclotron angular frequency (ω_c). This alteration of cyclotron angular frequency establishes the instability known as CRM instability. In the beam wave interactions, the cyclotron angular frequency of some electrons increases while

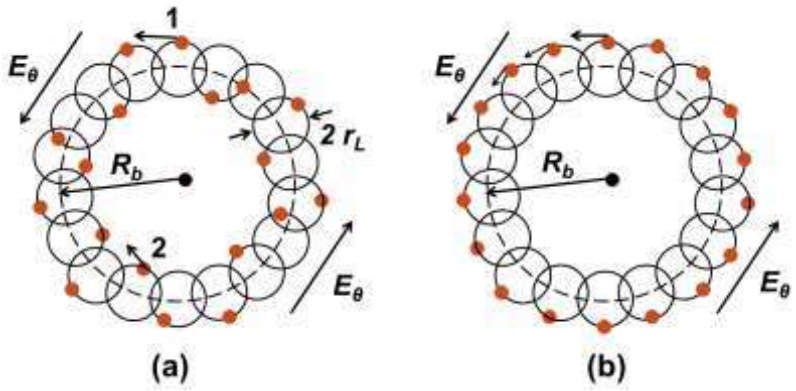

Figure 1.5 Illustration of phase bunching phenomenon in an annular electron beam (a) random distribution, and (b) phase bunched electrons in their cyclotron orbits.

the cyclotron angular frequency of some electrons decreases due to the transfer of energy and results in phase bunching of electrons [10]. The phase bunching process can be easily understood by assuming the zero axial velocity of the electron. To understand this, a beamlet is captured to analyze the process of phase bunching as shown in Figure 1.5 (a), where, B_o is the axial DC magnetic field. The electrons are arranged in annular circular orbits with radius r_L, typically r_L being much less than the beam radius R_b. Initially, the electrons are in a cyclotron orbit in a random manner as shown in Figure 1.5 (a). In TE_{mn} mode, electrons are accelerated or deaccelerated due to the RF electric field's transverse component. Apparently, there is no net energy transfer in the random phase of electrons [1], [25]. To understand the bunching process, two electrons in Figure 1.5 (a) are taken as electron 1 and 2. Due to the electric field's azimuthal component, the electron 1 deaccelerated and loses its energy, while electron 2 accelerated and obtains an equal amount of energy. Therefore, the relativistic mass (γm_e) of electron 1 decreases and electron 2 increases. Since then, the cryotron angular frequency of electron 1 is increased, and the cryotron angular frequency of electron 2 is decreased. As a result, the electrons form a bunch in the Larmor radius. This bunch of electrons transfers energy to RF wave if the wave frequency is slightly larger than the

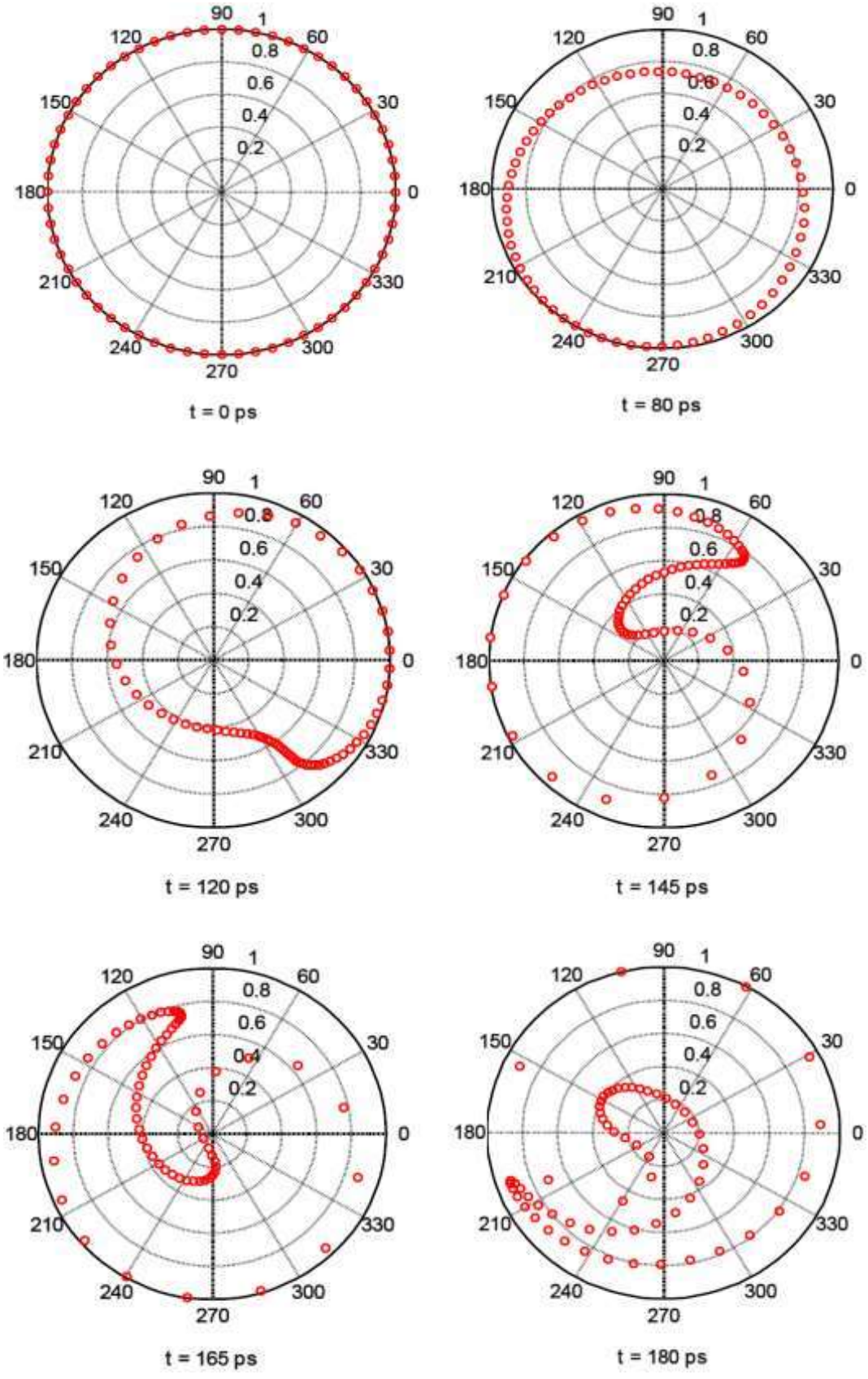

Figure 1.6 Time evolution of electrons phase distribution (shown as) on the Larmor orbit.

initial value of the cyclotron frequency as given by

$$\omega' - \frac{eB_o}{m_e \gamma_o'} > 0 \tag{1.4}$$

cyclotron angular frequency is inversely proportional to the relativistic mass as given in (1.3), electron 1 tends to gyrate faster than before, and electron 2 gyrate lower speed where, subscript 0 refers to the initial value and prime denotes the reference frame in which the electron axial velocity vanishes. Since, the cyclotron angular frequency of electron 1 increases as it comes closer to the resonance condition and loses more energy in the successive cycle. Similarly, the cyclotron angular frequency of electron 2 decreases as it goes far to the resonance condition and gain less energy in the successive cycle. Over the time, as the instability is further developed the energy of the wave grows and electrons bunch in phase within their cyclotron orbits as shown in Figure 1.5 (b). The phase bunching of the electrons during the CRM interaction is shown in Figure 1.6. These figures demonstrate the Larmor radii of electrons in the phase space as a function of time.

1.3.3. Operating Principle

For the beam-wave interaction process in a gyrotron oscillator, an electron beam is emitted from the cathode, which is guided from cathode to the gyrotron's collector in the presence of a DC magnetic field. As discussed earlier, the electron beam consists of several electrons that are gyrating around the lines of the magnetic field in a small helical path with a cyclotron angular frequency and whose frequency is very close to the operating frequency of the gyrotron they are moving towards the collector. These small helices are known as beamlets. As discussed earlier, transverse energy of the electron beam is extracted from the beam by relativistic CRM instability during beam-

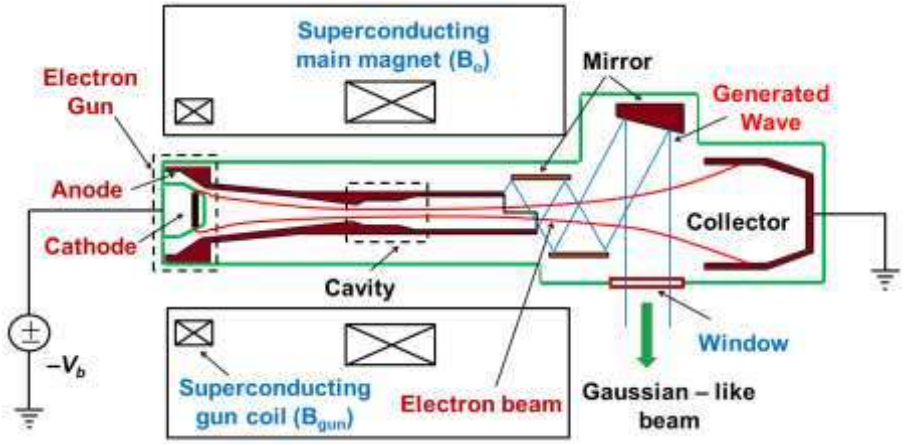

Figure 1.7 Schematic arrangement of a gyrotron oscillator [33].

wave interaction in gyrotrons. These bunches develop over time as well as the length of the interaction. If the operating frequency is slightly higher than the electron cyclotron frequency, the bunches slip into the RF field phase and fall into the retarding phase, resulting in the transfer of energy from the beam to the RF wave [32]. After the beam–wave interaction, the spent electron beam is eventually collected by a thermally cooled collector.

1.3.4. Schematic and Working

A schematic of gyrotron oscillator including its sub-assemblies is shown in Figure 1.7. It consists of a magnetron injection gun (MIG) that produces an annular electron beam, a thin cylindrical RF interaction cavity surrounded by a superconducting magnet, and an RF extraction region [25]. Two anodes are present in the triode type MIG. In the MIG, the electron beam is formed by the conical-shaped thermionic cathode surface, which is based on the heating of the emitting surface to allow electrons to conquer the work function and break out of the surface. The most frequent incubation-emitting types of dispensers are LaB_6, scandate, and thorium-based cathodes. A pulsed or continuous potential is applied to the first anode of the MIG. Electrons are emitted from the annular strip of the conical-shaped cathode's lateral face

at a pre-fixed angle decided by the pitch factor (α). The pitch factor is determined by the ratio of transverse velocity $(v_{\perp})$ to the axial velocity(v_z). Generally, the pitch factor α is chosen between 1 and 2 for a gyrotron oscillator. The electric field is perpendicular to the magnetic field generated by the gun solenoid in the area between the cathode and the first anode. The second anode supplies the axial energy to the electron beam. Electrons acquire both orbital and axial velocity components at the end of the cathode-anode region and gyrate helically about a fixed guiding center. The beam radius remains annular and maintains its path in the Larmor radius as it propagates along the interaction region. Magnetic fields increase from the gun region to the interaction region; therefore, due to the magnetic field's adiabatic invasion, the electron orbital momentum increases. In the RF interaction field, the magnetic field is kept uniform. The electron beam interacts with the desired mode and RF noise at the interaction region's supportive frequency.

Usually, the RF interaction structure of gyrotron involves a smooth wall, open-ended tapered cylindrical resonator [1], [9], [34]. Generally, the RF interaction structure is divided into three sections: the down-taper, straight middle section, and the up-taper. The down-taper is like a hollow cone whose radius decreases towards the gun and increases towards the middle part of the interaction structure. The down-taper prevents the back-propagation from coming the middle section towards the electron gun. The radius of the middle section of the RF interaction structure remains uniform, where the intensity of the RF field achieves its maximum value. The up-taper section provides the facility the conversion of the standing wave into the traveling wave to couple out from the RF interaction structure. The RF cavity's design parameters are optimized so that the RF field intensity is maximum at the mid of the straight section and no mode conversion

occurs in the cavity. Sometimes, parabolic smoothing is used to avoid the mode conversion at the joint of the sections.

After the beam-wave interaction occurs, the grown RF signal is extracted from the cavity by using an RF window that provides a vacuum seal to the RF cavity. The low-loss vacuum grade dielectric material is used to design the RF window. In the case of radial extraction, the RF output power is converted into a Gaussian beam using a mode converter before the extraction through the RF window. Finally, the spent electron beam is collected at the collector. In practice, a large fraction of the electron beam's energy remains lively and converted into heat at the collector. Hence, an energy recovery system is used to enhance the efficiency of the device significantly. The depressed collector is used to improve the efficiency for the gyrotron [35].

1.4. Dynamic Nuclear Polarization / Nuclear Magnetic Resonance

Nuclear Magnetic Resonance (NMR) spectroscopy is one of the most promising spectroscopy approaches to solve problems in physics, chemistry, biology, medicine, physics, structural studies of macro-molecular biological systems-proteins, and nucleic acids due to its excellent resolution [36] – [37]. The resolution in the NMR experiment increases by increasing the NMR magnetic field, as a result, the NMR frequency also increases. The higher resolution in the NMR experiment is the result of longer atomic relaxation times that are obtained due to the small magnetic moments of the atom that couples weakly to the surrounding lattice. However, the small size of these magnetic moments in NMR experiments reduces sensitivity. Dynamic Nuclear Polarization (DNP) is a technique that increases the sensitivity by transferring large electron spin polarization from the stable paramagnetic center to the nuclear reservoir (nuclear spin) in the NMR experiment [27]. The DNP has improved the sensitivity in NMR

experiments by a factor of 20 to 400, depending upon the experimental conditions such as the temperature, solvent composition, deformation level, radical type and concentration [38] – [39]. For ^{1}H spins, the theoretical maximum enhancement in the signal intensity of the NMR experiment is given by the relationship $\gamma_s / \gamma_i \sim 660$, where γ_s and γ_i are the electron and nuclear gyromagnetic ratios. A high-frequency (0.1 – 1 THz) source is required in DNP technique, which is irradiated at electron Larmor frequency and interacts with magnetized electron spins, via quantum-mechanical couplings into nuclear spins and significantly increases the NMR signal intensity [27]. Therefore, the DNP technique requires a microwave source with wide tuneable bandwidth to optimize the frequency matching conditions between the nuclear spin and electron spin.

1.5. DNP / NMR Gyrotrons

The theoretical discussion of cyclotron maser interactions began in the 1950s itself, and later the gyrotron was recognized as one of the promising sources of high-power millimeter wave radiation [1]. Electron-cyclotron- resonance-heating (ECRH), electron-cyclotron-current-drive (ECCD) and DNP / NMR are among the foremost applications of gyrotrons that have driven the evolution of gyrotrons for the past several decades [40] - [41]. Fusion in the ITER tokamak had to rely on other external heat sources to bring the plasma temperature to ~150 million 0C [42] - [43]. In the present ECRH system, 110 GHz to 170 GHz gyrotrons play a key role in generating sufficient power[44]-[45]. Countries like Russia (GYCOM), the United States (CPI), Germany (EU) and Japan (JAERI) have extensively focused on 110-170 GHz megawatts gyrotrons [15]-[16], [46]-[50]. Forschangszentrum Karlsruhe developed in a first step a 140 GHz gyrotron for output power 500 kW with efficiency 31% [51]-[53]. Many labs

like KIT (Karlsruhe Institute of Technology and CPI (Communications & Power Industries) have been trying to be developing for years an MW gyrotron at 140 GHz [41], [54]. Recently, ECRH & CD applications required a 24MW of the long pulse (~3600 s) RF power at 170GHz and for this, the ITER Tokamak in France has planned to generate 241 MW gyrotron system [55]-[56]. Further, high frequency (0.24 THz) gyrotron are expected to produce about 1 MW output power for ECRH & CD in DEMO [57]-[58]. The present thesis is focused on the low-power tuneable gyrotron for DNP / NMR spectroscopy applications.

The first ever gyrotron for DNP / NMR spectroscopy application was developed at Francis Bitter Magnet Laboratory, Massachusetts Institute of Technology (MIT), USA, in 1993 by Becerra *et al.*, which has generated a CW output of ~20 W at 140 GHz with 5 T magnetic fields [59]. Subsequently, a gyrotron was demonstrated for several hundred of watts in a submillimeter regime using high energy beams at the research center for the development of the Far-Infrared Region of the University of (FIR-FU), Japan [60]–[61]. In 2003, a gyrotron was developed at 250 GHz for higher NMR frequency with a tuneable bandwidth of ~1.8 GHz in the span of 5.8 T – 9 T [62]. After a decade, another 250 GHz gyrotron at MIT, USA, with an improved tuneable bandwidth of ~3 GHz was experimentally tested by varying both beam voltage (V_b) and magnetic field [63] and simultaneously a 260 GHz gyrotron was tested for its tunability by varying only magnetic field at Centre de Recherches en Physique des Plasmas - Ecole Polytechnique operation such as 10–22 T Nb_3Sn superconductive magnets, gyrotron is operated in high-harmonic with a low cost of 10 T N_bT_i superconductive magnets [69]. During the last decade, to achieve impressive achievements in DNP / NMR applications, a series of high-harmonic THz gyrotrons are successfully

Table 1.1: State-Of-The-Art of the DNP/NMR gyrotrons

S. No.	Frequency/ Mode	Lab	Author/ Year	Power/ Bandwidth
1	140 GHz	Massachusetts Institute of Technology, Cambridge, Massachusetts	Becerra *et al.* 1993	20 Watt
2	394 GHz for TE_{04}, TE_{09}, TE_{81}	Department of Applied Physics, Faculty of Engineering. Fukui University. Fukui 910, Japan.	Idehara *et al.* 1995	few tens of Watt
3	250 GHz $TE_{0,3}$	Francis Bitter Magnet Laboratory, Department of Chemistry, Massachusetts Institute of Technology.	Bajaj *et al.* 2003	10- 15 W,
4	460 GHz, $TE_{2,6}$	Plasma Science and Fusion Center, Massachusetts Institute of Technology, Cambridge, USA.	Hornstein, *et al.* 2005	70 W
5	140 GHz, TE_{03}	The Plasma Science and Fusion Center, Massachusetts Institute of Technology, Cambridge, USA	Joye *et al.* 2006	14W
6	394.3 GHz,TE_{06}	Research Center for Development of Far Infrared Region, University of Fukui, Japan	Idehara *et al.* 2007	30 W (Second harmonic)
7	460 GHz, TE_{06}	Plasma Science and Fusion Center, MIT, Cambridge, USA,	Hana *et al.* 2007	Simple cylindrical, 8 W
8	460 GHz, TE_{43}	Plasma Science and Fusion Center, MIT, Cambridge, USA,	Torrezan *et al.* 2011	2-18 W, 1.2 GHz
9	400 GHz, TE_{06}	Research Center for Development of Far Infrared Region, University of Fukui, Japan.	Idehara *et al.,* 2010	10 W
10	460 GHz, $TE_{11,2}$	Plasma Science and Fusion Center, Massachusetts Institute of Technology, Cambridge, USA.	Torrezan *et al.* 2000	16 W, (Second harmonic)
11	330 GHz, TE_{43}	Plasma Science and Fusion Center, Massachusetts Institute of Technology, Cambridge, USA.	Torrezan *et al.* 2011	Complex Cavity, 18 W, 1 GHz, 0.90%
12	260 GHz, TE_{72}	Centre de Recherches en Physique des Plasmas, Ecole Polytechnique F ed erale de Lausanne (CRPP-EPFL), Lausanne, Switzerland	Alberti *et al.* 2012	Simple cavity, 152 W, 1.2 GHz
13	250 GHz, TE_{52}	Plasma Science and Fusion Center, Massachusetts Institute of Technology, Cambridge, USA.	Barnes *et al.* 2012	Simple cylindrical, avg. power > 35 W, 3 GHz
14	527 GHz, TE15,3	Communications and Power Industries, LLC Palo Alto, USA	Felch *et al.,* 2013	Simple cylindrical, avg. power 25 W
15	263 GHz, TE_{53}	Institute of Applied Physics, Russia	Glyavin *et al.,* 2015	1 kW
16	460GHz, $TE_{8,5}$	Research Center for Development of Far-Infrared Region, University of Fukui (FIR UF), Bunkyo	Idehara *et al.,* 2015	1 kW (Second harmonic)
17	0.79 THz, $TE_{8,5}$	Research Center for Development of Far-Infrared Region, University of Fukui, Fukui 910-8507, Japan	Idehara *et al.,* 2017	1 kW (Second harmonic)
18	527 GHz, $TE_{11,2}$	Plasma Science and Fusion Center, Massachusetts Institute of Technology, Cambridge, USA.	Jawla *et al.,* 2020	10 W, 0.35 GHz

demonstrated in various organizations including MIT, USA [70]–[74], Institute of Applied Physics, Russian Academy of Sciences (IAP, RAS), Russia [75], Fukui University (Japan) [76]–[79]. The state-of-the-art gyrotron for DNP/NMR applications is described in Table – 1.1 along with the respective lab with frequency, operating mode, output power, and tunable bandwidth.

1.6. Current Effort

Significant improvement in the performance of the tuneable gyrotrons operating in fundamental and second harmonic mode is achieved in the recent past for the DNP / NMR applications as given in Table - 1.1. The higher resolution in the NMR experiment requires a microwave source which operate at higher frequency. Barnes *et al.* have demonstrated a gyrotron operating in fundamental mode at ~250 GHz for 380 MHz NMR spectrometer with tuneable bandwidth ~3 GHz. Alberti *et al.* have demonstrated a gyrotron operating in fundamental mode at ~260 GHz for 400 MHz NMR spectrometer with tuneable bandwidth ~1.2 GHz. The latter gyrotron provide the higher resolution in the NMR experiment among all the experimentally demonstrated gyrotrons [Table - 1.1], those operating in the fundamental mode. But, the tuneable bandwidth of the ~260 GHz gyrotron is low as ~1.2 GHz. The present research's motivation is to improve the tuneable bandwidth of the ~260 GHz gyrotron for the ~400 MHz NMR spectroscopy applications.

The present thesis aims to enhance tunable bandwidth of 260 GHz gyrotron for a 400 MHz NMR spectrometer by using magnetic/thermal tuning schemes, a selective mode structure in the form of an RF interaction circuit, and a multi-section slightly tapered cavity of the gyrotron. The Particle-In-Cell (PIC) simulation is performed to observe the above-mentioned cavity-based gyrotron's beam-wave interaction behavior.

In order to validate the PIC simulation results, a code is developed by revisiting the Multimode analytical theory. Thermal tuning is performed by controlling the thermal deformation of the RF cavity by varying the coolant temperature. Since the thermal tuning scheme is independent of the magnetic tuning scheme, the total tuneable bandwidth of gyrotron is the superposition of the individual tuneable bandwidth achieved by both the thermal and the magnetic tuning schemes.

The tuneable bandwidth of the gyrotron can be enhanced by using a highly mode selective circuit, Photonic Band Gap (PBG) structures as an RF interaction circuit. The PBG cavity is realized by creating a defect in 2D triangular lattice of the PBG structure. The PBG cavity is designed and tuned to confine the desired operating mode with higher Q-factor than other competing modes. Therefore, the operating mode has strong coupling to the electron beam; consequently, the tuneable bandwidth of the PBG cavity-based gyrotron is enhanced. The ohmic loss effect is less in the PBG cavity-based gyrotron due to its larger transverse dimension compared to the conventional gyrotron. Therefore, the PBG gyrotron provides a stable operation as compared to conventional gyrotrons.

Further, the tuneable bandwidth is enhanced by modifying the conventional gyrotron's three-section cavity into a slightly tapered multi-section cavity. The diffractive Q-factor is remarkably maintained by using multi-section slightly tapered cavity even operating in higher-order axial mode number; hence the tuneable bandwidth is enhanced. Finally, the simulation investigation of second-harmonic ~527 GHz gyrotron for 800 MHz NMR spectrometer is investigated by using the Multimode theory. The tuneable bandwidth of the sub-millimeter-wave gyrotron is studied using a magnetic tuning scheme, and its tuneability is further enhanced by using the thermal tuning scheme.

1.7. Plan and Scope

The tunable microwave source requirement in millimeter, submillimeter-wave, and THz regime for DNP / NMR spectroscopy applications has motivated the author to carry out the work embodied in the present thesis. The current work explored the enhancement of the gyrotron's tunable bandwidth by using different techniques, including thermal tuning, using PBG structures, and a multi-section slightly tapered cavity as the RF interaction circuit gyrotron.

In the present chapter, the current work's motivation has been devised, in which the problems of high-frequency operation of a tuneable microwave source for DNP / NMR applications are described. Gyrotron has been proposed as a possible solution for diagnosing these problems because, which can produce a few tens of Watt CW power in millimeter, sub-millimeter wave, and THz regime for a long time period as compared to other microwave sources. The basics of the microwave vacuum electronic devices and their applications, and the evolution of microwave sources and their limitations have been discussed. The classification of microwave tubes and particularly the operating principle of gyrotron oscillator in terms of the dispersion relation, instabilities, CRM interaction and phase bunching mechanism have been elaborated. Before summarizing the plan and scope of the present thesis, the literature survey of tunable gyrotron has been made and presented.

In Chapter 2, the nonlinear Multimode theory has been explored and revisited to investigate the gyrotron's beam-wave interaction behavior. Initially, the gyrotron oscillator's design methodology has been studied along with various constraints in selecting the design parameters. The developed Multimode code has been used to compute the output power in the desired operating mode and its competing modes for any guided and open structures like PBG cavity and confocal cavity. The present

Multimode calculation is performed by assuming a thin annular electron beam instead of an experimental guiding centered beam. The space charge effect of the electron beam is assumed to be negligible. The fixed Gaussian or sinusoidal axial profile is assumed for each mode in the Multimode calculation. The Multimode results are numerically benchmarked against the published experimental results.

Chapter 3 deals with the PIC simulation studies and their validation with Multimode studies of the gyrotron discussed in Chapter 2. The beam-wave interaction behavior has been presented using the PIC solver module of the commercially available tool "CST Particle Studio". Both thermal and structural analyses have been performed by using Fluent Solver and Static Structural solver in the ANSYS, respectively. The magnetic tuning has been performed to achieve the tuneable bandwidth of the gyrotron. The tuneable bandwidth has been further enhanced by using the thermal tuning scheme. In addition, the design of RF window and collector has also been described.

Chapter 4 includes the design of a metal PBG cavity for a tunable gyrotron as its RF interaction circuit. The dispersion relation and global band diagram have been calculated by using a unit cell of 2D triangular lattice of PBG structures. The cold analysis has been performed to observe the transient behavior and electromagnetic behavior of the PBG cavity. PIC simulation has been used to calculate the output power and resonating frequency and the obtained results are also validated to the Multimode simulation results. Magnetic tuning has been used to achieve the tuneable bandwidth of the gyrotron. The thermal analysis has been performed by using "CST Mphysics" and ANSYS.

In Chapter 5, a multi-section slightly tapered cavity has been designed by modifying the straight section of the conventional gyrotron's three-section cavity, as discussed in Chapter 3. The diffractive Q-factor (Q_d) and resonating frequency, ω_r are

estimated by using the minimization method. The design parameters are optimized by observing their effect on Q_d and ω_r. The magnetic and thermal tuning scheme are used to achieve the tuneable bandwidth of the gyrotron.

In Chapter 6, a second harmonic gyrotron has been modeled to operate in a submillimeter-wave regime. The Multimode analysis of the second-harmonic gyrotron has been done to calculate the RF output power in the desired operating mode along with its competing modes. The Multimode results have been validated to the published experimental results. The magnetic tuning is performed to achieve the tuneable bandwidth by using the Multimode code. The tuneable bandwidth has further been enhanced by using the thermal tuning scheme.

In Chapter 7, the works embodied in the present thesis are summarized. The conclusion of the present thesis is made. Finally, the limitations and future scope of the present work are outlined.